



Article

Cost Effective Solvothermal Method to Synthesize Zn-Doped TiO₂ Nanomaterials for Photovoltaic and Photocatalytic Degradation Applications

Tharmakularasa Rajaramanan ^{1,2}, Sivagowri Shanmugaratnam ^{1,2}, Vijayakumar Gurunathanan ¹, Shivatharsiny Yohi ³, Dhayalan Velauthapillai ^{2,*}, Punniamoorthy Ravirajan ¹ and Meena Senthilnathanan ^{3,*}

¹ Clean Energy Research Laboratory (CERL), Department of Physics, University of Jaffna, Jaffna 40000, Sri Lanka; rramanan9@gmail.com (T.R.); Sivagowrishanmugaratnam@gmail.com (S.S.); guru201666@gmail.com (V.G.); pravirajan@univ.jfn.ac.lk (P.R.)

² Faculty of Engineering, Western Norway University of Applied Sciences, 5020 Bergen, Norway

³ Department of Chemistry, University of Jaffna, Jaffna 40000, Sri Lanka; yshiva@univ.jfn.ac.lk

* Correspondence: Dhayalan.Velauthapillai@hvl.no (D.V.); meena@univ.jfn.ac.lk (M.S.); Tel.: (+47)-55-58-77-11 (D.V.); (+94)-212218193 (M.S.)

Abstract: Titanium dioxide (TiO₂) is a commonly used wide bandgap semiconductor material for energy and environmental applications. Although it is a promising candidate for photovoltaic and photocatalytic applications, its overall performance is still limited due to low mobility of porous TiO₂ and its limited spectral response. This limitation can be overcome by several ways, one of which is doping that could be used to improve the light harvesting properties of TiO₂ by tuning its bandgap. TiO₂ doped with elements, such as alkali-earth metals, transition metals, rare-earth elements, and nonmetals, were found to improve its performance in the photovoltaic and photocatalytic applications. Among the doped TiO₂ nanomaterials, transition metal doped TiO₂ nanomaterials perform efficiently by suppressing the relaxation and recombination of charge carriers and improving the absorption of light in the visible region. This work reports the possibility of enhancing the performance of TiO₂ towards Dye Sensitised Solar Cells (DSSCs) and photocatalytic degradation of methylene blue (MB) by employing Zn doping on TiO₂ nanomaterials. Zn doping was carried out by varying the mole percentage of Zn on TiO₂ by a facile solvothermal method and the synthesized nanomaterials were characterised. The XRD (X-Ray Diffraction) studies confirmed the presence of anatase phase of TiO₂ in the synthesized nanomaterials, unaffected by Zn doping. The UV-Visible spectrum of Zn-doped TiO₂ showed a red shift which could be attributed to the reduced bandgap resulted by Zn doping. Significant enhancement in Power Conversion Efficiency (PCE) was observed with 1.0 mol% Zn-doped TiO₂ based DSSC, which was 35% greater than that of the control device. In addition, it showed complete degradation of MB within 3 h of light illumination and rate constant of $1.5466 \times 10^{-4} \text{ s}^{-1}$ resembling zeroth order reaction. These improvements are attributed to the reduced bandgap energy and the reduced charge recombination by Zn doping on TiO₂.

Keywords: doped TiO₂; zinc; solvothermal method; DSSCs; MB



Citation: Rajaramanan, T.; Shanmugaratnam, S.; Gurunathanan, V.; Yohi, S.; Velauthapillai, D.; Ravirajan, P.; Senthilnathanan, M. Cost Effective Solvothermal Method to Synthesize Zn-Doped TiO₂ Nanomaterials for Photovoltaic and Photocatalytic Degradation Applications. *Catalysts* **2021**, *11*, 690. <https://doi.org/10.3390/catal11060690>

Academic Editor: Giuseppina Pinuccia Cerrato

Received: 30 April 2021

Accepted: 27 May 2021

Published: 29 May 2021

Publisher's Note: MDPI stays neutral with regard to jurisdictional claims in published maps and institutional affiliations.



Copyright: © 2021 by the authors. Licensee MDPI, Basel, Switzerland. This article is an open access article distributed under the terms and conditions of the Creative Commons Attribution (CC BY) license (<https://creativecommons.org/licenses/by/4.0/>).

1. Introduction

The global population is increasing rapidly, and the limited supply of nonrenewable energy leads to rising energy demands, especially in developing countries. This risks the depletion of cheap fossil energy sources and an increase in environmental pollution as well as climate change [1]. Hence, researchers around the world were constantly inventing solutions to expand the energy sources and reduce greenhouse gas emissions. This took renewable energy sources into the spotlight [2]. Renewable energy sources such as solar, wind, geothermal, hydropower, biofuel, and biomass are considered to be cleaner and more environmentally friendly sources of power. However, energy production from these

alternative energy sources is yet restricted because of high production costs and poor energy conversion efficiency. Nanotechnology is increasingly playing an active role in overcoming the above limitations [3,4].

Titanium dioxide (TiO₂) was widely used as a golden standard nanomaterial for sustainable energy generation and the removal of environmental pollutants [5,6] due to its efficient photocatalytic activity, low cost, nontoxic nature and high stability [7]. Although TiO₂ exhibits the desired performance in ultraviolet light, its overall performance is still limited because of low mobility of porous TiO₂ [8] and its limited spectral response wide bandgap (3.0–3.2 eV) that cannot make use of visible light [9]. Several strategies were investigated and reported to overcome this limitation, which include preparation of nanocomposites [10–12], doping/codoping [5,13,14], and synthesis of particles with different nanostructures [15,16], such as nanorods, nanowires, nanotubes, etc. Among these strategies, doping/co-doping displays major impacts on the band structure and trap states of TiO₂, and hence, alters its properties such as conduction band energy, charge transport, recombination, and collection significantly [17]. Even though nonmetals, alkali-earth metals, and rare-earth elements are being used as dopants, transition metal doped TiO₂ nanomaterials are notable candidates for photovoltaic and photocatalytic degradation applications as they improve absorption in the visible region and suppress relaxation and recombination of charge carriers [13].

Zinc (Zn) is one of the promising n-type transition metals; it improves the photocurrent of Dye Sensitized Solar Cell (DSSC) when incorporated with TiO₂ [18]. It also enhances the photocatalytic activity in visible region [19] by reducing the bandgap of TiO₂ [20,21]. Zhu et al. demonstrated the photovoltaic analysis of hydrothermally synthesized Zn-doped TiO₂ photoanode, and their findings reveal that incorporation of Zn²⁺ ions into an anatase lattice of TiO₂ elevates the edge of conduction band (CB) of the photoanode and the Fermi level is shifted towards the CB edge, which contributes to the improvement in open-circuit voltage (V_{OC}), and thus, enhanced photovoltaic performance [22]. Huang et al. reported that the device fabricated with Zn-doped TiO₂ nanomaterials, synthesized by agarose gel method, shows better photovoltaic performance due to the improved short circuit current density (J_{SC}) [18]. Zn-doped TiO₂ is widely used in photocatalysis as well. Zhao et al. analyzed the photocatalytic degradation of Rhodamine B dye using Zn-doped TiO₂, synthesized by hydrogen–oxygen diffusion flame method, where Zn doping creates appropriate energetic position between ZnO and the excited state of dye molecule, which enhances the electron injection into the conduction band of TiO₂ by capturing electrons, and subsequently promotes the formation of reactive oxygen species which enhances the degradation process [20]. Chen et al. demonstrated the degradation of Methyl orange by Zn-doped TiO₂ synthesized by stearic acid gel method, and higher photocatalytic activity was achieved due to greater BET surface area by Zn doping [23]. Zn-doped TiO₂ was synthesized using facile sol-gel reflux method by Tariq et al., and the synthesized nanomaterials were used to degrade methylene blue (MB) and methyl orange dyes. Here, Zn acted as a reductant to facilitate the Ti³⁺ formation and a stabilizer for the oxygen vacancies [21]. Hence, Zn effectively modified the properties of TiO₂ and improved the degradation of dye molecules.

The doped TiO₂ nanomaterials can be synthesized by different methods including hydrothermal synthesis [22], solvothermal synthesis [24], spray pyrolysis [25], microwave synthesis [26], and spin coating [27]. However, hydrothermal and solvothermal methods are preferable, as high crystalline nanomaterials are formed in these syntheses which leads to uniform particle distribution [28]. Although several studies reported on photovoltaic and photocatalytic activities of Zn-doped TiO₂, the present study reports a simple solvothermal synthesis of Zn-doped TiO₂ nanomaterials utilizing cost effective reaction bottles instead of autoclave followed by characterization of the same, and investigates their efficiency on photovoltaic and photocatalytic degradation applications.

2. Results and Discussion

The Zn-doped and undoped TiO₂ nanomaterials, synthesized by a simple solvothermal method, were structurally and optically characterized utilizing XRD, EDX (Energy Dispersive X-ray), and UV-Visible spectroscopies, and their photovoltaic and photocatalytic degradation activity were studied.

2.1. X-ray Diffraction (XRD) Spectroscopy

The diffraction pattern and crystal structure of the synthesized, undoped, and 0.5, 1.0, 1.5, and 2.0 mol% Zn-doped TiO₂ nanomaterials were examined by XRD, as illustrated in Figure 1. For XRD analysis, the powder sample was placed on a microscopic glass plate and pressed by another glass plate to obtain thin layer of the sample. The peaks attained at the 2θ values of 25.2°, 37.6°, 48.2°, 53.7°, 55.0°, 62.5°, 68.5°, 70.2°, 74.8°, and 82.5° correspond to the reflection planes of (101), (004), (200), (105), (211), (204), (116), (220), (215), and (224), respectively. The observed peaks, corresponding to only anatase phase of TiO₂, for all undoped and Zn-doped TiO₂ nanomaterials indicate that incorporation of Zn on TiO₂ did not influence phase transformation. This may be attributed to the similar ionic radii of Ti⁴⁺ (0.74 Å) and Zn²⁺ (0.605 Å) ions [29] which allow Zn²⁺ ions to be easily accommodated on to the TiO₂ lattice without altering their crystal structure.

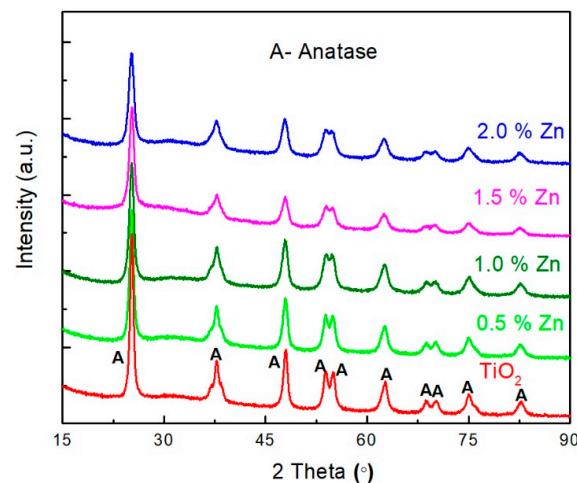


Figure 1. X-Ray Diffraction (XRD) patterns of the undoped and Zn-doped TiO₂ nanomaterials.

The average crystalline size of the synthesized nanomaterials was estimated by Debye–Scherrer equation using the predominant anatase (101) plane.

$$d = \frac{k\lambda}{\beta \cos\theta} \quad (1)$$

where, *d* is the average crystalline size of the particles, *k* is the dimensionless shape factor which has a typical value of about 0.89, *λ* is the wavelength of the X-ray beam (0.5406 nm), *θ* is the Bragg angle, and *β* is the full width at half maxima (FWHM), and is calculated from the predominant anatase (101) plane. The estimated crystalline sizes were about 12, 10, 9, 8, and 7 nm for undoped, 0.5, 1.0, 1.5, and 2.0 mol% Zn-doped TiO₂ nanomaterials, respectively. These results demonstrate that Zn doping reduces the crystalline size of nanomaterials. Huang et al. supported this observation by reporting that Zn–O–Ti bonds are formed during the doping of Zn on TiO₂, which inhibit the growth of crystal grains of TiO₂ and subsequently reduce the size of particles [18]. The lattice strain of the nanomaterials was calculated using Williamson–Hall (W–H) plot method.

$$\beta \cos\theta = \epsilon 4 \sin\theta + \frac{0.9\lambda}{d} \quad (2)$$

where, λ is the wavelength of X-ray radiation, β is FWHM, and θ is the Bragg angle of the diffraction peaks, d is the crystallite size with lattice strain, and ε is the effective value of the lattice strain. $\beta \cos \theta$ is plotted against $4 \sin \theta$, and after linear fitting, the slope gives the value of lattice strain [30,31]. The values of the lattice strain are 7.53×10^{-5} , 1.16×10^{-4} , 5.38×10^{-4} , -0.00499 , and -0.00296 for the undoped, and 0.5, 1.0, 1.5, and 2.0 for the mol% Zn-doped TiO₂ nanomaterials, respectively. Positive lattice strain value indicates that the system is under tensile strain, and negative value indicates that the system is under compressive strain [32]. Lattice strain of the 1.0 and 0.5 mol% of Zn-doping is higher than undoped TiO₂ due to the reduced crystalline size, and the values are negative for the 1.5 and 2.0 mol% of Zn doping [32,33]. The formation of ZnO in the higher Zn doping may cause distortion, which might be the reason for the negative value. Further, the absence of peaks for Zn in the XRD of Zn-doped TiO₂ nanomaterials may be attributed to the very small quantity of Zn doped on TiO₂ and homogeneous dispersion of Zn on TiO₂; the same was reported by Yanqi et al. [34] and Feng et al. [22].

2.2. Energy Dispersive X-ray (EDX) Spectroscopy

The existence of Zn in the Zn-doped TiO₂ nanomaterials was confirmed by EDX analysis, as shown in Figure 2. The summary of EDX results, presented in Table 1, confirms that the amount of Zn doped in TiO₂ rises with the increase in Zn dopant used for the synthesis of Zn-doped TiO₂ nanomaterials, and the distribution of Zn dopant in TiO₂ is found to be uniform.

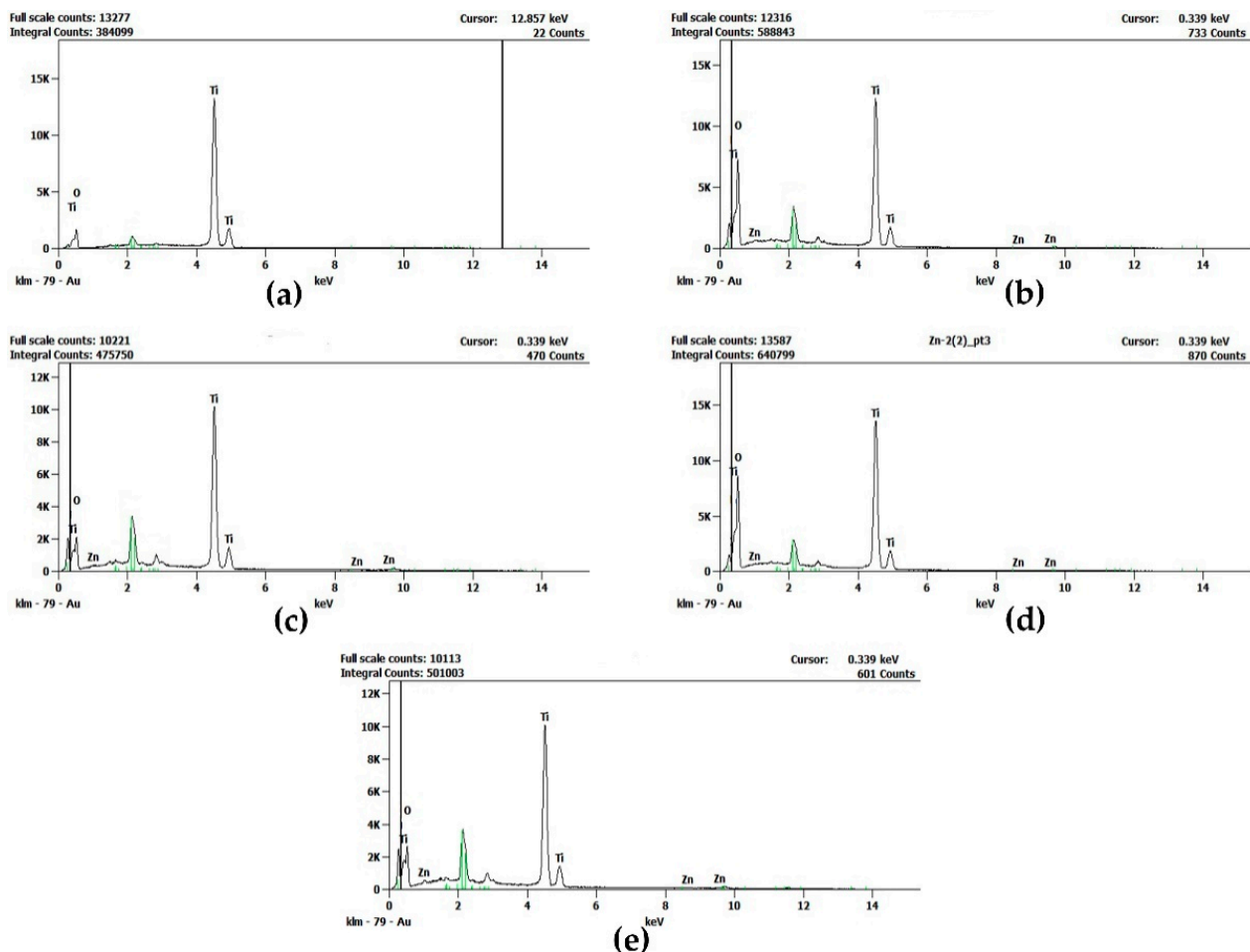


Figure 2. Energy Dispersive X-ray (EDX) spectroscopic images of (a) undoped, (b) 0.5 mol% Zn-doped, (c) 1.0 mol% Zn-doped, (d) 1.5 mol % Zn-doped, and (e) 2.0 mol% Zn-doped TiO₂ nanomaterials.

Table 1. Mole percentage of Zn in Zn-doped TiO₂ nanomaterials.

Sample	mol% of Zn Dopant (from EDX Results)
Undoped TiO ₂ (a)	-
0.5 mol% Zn-doped TiO ₂ (b)	0.5
1.0 mol% Zn-doped TiO ₂ (c)	0.8
1.5 mol% Zn-doped TiO ₂ (d)	1.3
2.0 mol% Zn-doped TiO ₂ (e)	1.7

2.3. UV-Visible Spectroscopy

To study the optical properties of the Zn-doped and undoped TiO₂, the powder samples were coated on the microscopic glass plate by doctor-blade method and analyzed by UV-visible spectroscopy, as shown in Figure 3. Zn doping in TiO₂ led to a red-shift in the UV-visible light absorption of TiO₂ and the shift moved towards longer wavelength when the Zn content increased in the Zn-doped TiO₂ nanomaterials.

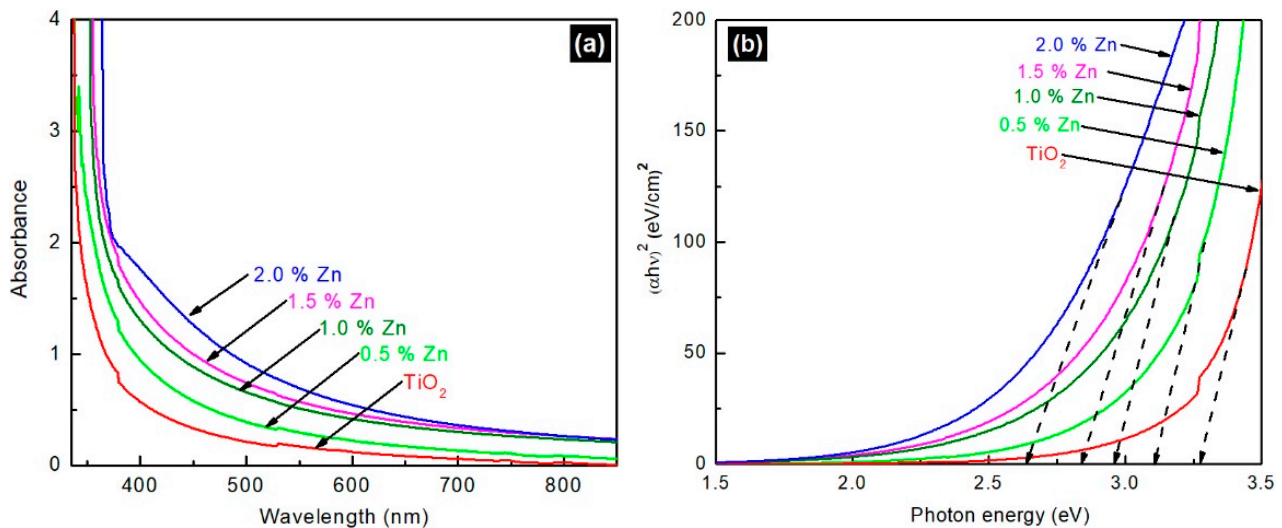


Figure 3. (a) UV-visible absorption spectra of undoped and Zn-doped TiO₂ nanomaterials; (b) Tauc-plot on estimated bandgap values of undoped and Zn-doped TiO₂ nanomaterials.

The Tauc's formula, given below, was used to estimate the bandgap of the films from UV-visible Spectra:

$$\alpha = A \frac{(h\nu - E_g)^n}{h\nu} \quad (3)$$

where α is the absorbance coefficient, $h\nu$ is the photon energy, A is a constant, E_g is the bandgap energy, and n is the exponential constant index which depends on the nature of transition ($n = \frac{1}{2}$ and 2 for indirectly and directly allowed transitions, respectively). The estimated bandgap values obtained from Tauc-plot are 3.3, 3.1, 3.0, 2.9, and 2.7 eV for the undoped, 0.5, 1.0, 1.5, and 2.0 mol% Zn-doped TiO₂, respectively. The above bandgap values, which reveal Zn-doping in TiO₂ reduces the bandgap of TiO₂, are in good agreement with the theoretical values reported by the Wang et al. [35] and experimental trends reported by Arunachalam et al. [36] and Aware et al. [37]. It is noteworthy that observations contradictory to the present study were also reported in literature [22].

2.4. Photovoltaic Measurement

2.4.1. J-V Measurement

The photovoltaic performance of the fabricated DSSCs with undoped and Zn-doped TiO₂ photoanodes was tested under simulated irradiation of intensity 100 mW/cm² with

Air Mass (AM) 1.5 filter. The results are illustrated in Figure 4, and the related photovoltaic parameters are summarized in Table 2.

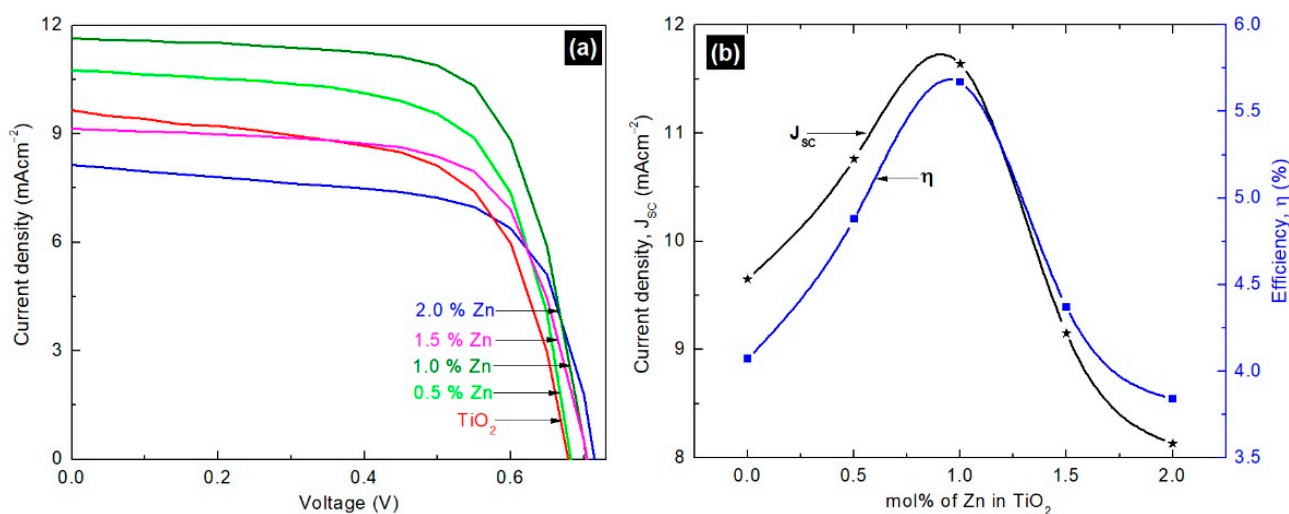


Figure 4. (a) Photovoltaic performances of Dye Sensitized Solar Cells (DSSCs) with undoped and Zn-doped TiO₂ photoanodes; (b) variations in short circuit current density (J_{sc}) and efficiency (η) with different mol% Zn dopants under illumination of intensity 100 mWcm^{-2} with Air Mass (AM) 1.5 filter.

Table 2. Photovoltaic parameters of DSSCs with undoped and Zn-doped TiO₂ photoanodes under illumination of intensity 100 mWcm^{-2} with AM 1.5 filter.

Zn (mol%)	J_{sc} (mAcm ⁻²)	V_{OC} (V)	FF	η
0.0	9.65	0.67	0.62	4.07
0.5	10.76	0.68	0.66	4.88
1.0	11.64	0.70	0.69	5.67
1.5	9.15	0.70	0.68	4.37
2.0	8.13	0.71	0.66	3.84

The results reveal improved J_{sc} , open circuit voltage (V_{OC}), and fill factor (FF) values for DSSCs fabricated with 0.5 and 1.0 mol% Zn-doped TiO₂ compared to that of the control device. The FF value increased up to 0.69 for the device made with 1.0 mol% Zn-doped TiO₂, followed by a reduction to 0.66 for the one made with 2.0 mol% Zn dopant. The V_{OC} sequentially increased from 0.67 to 0.71 V with increase in Zn content in the Zn-doped TiO₂. Nevertheless, the performance of the device, η , was mainly dominated by its J_{sc} value (as illustrated in Figure 4 (b)). The observed highest J_{sc} value of 11.64 mAcm^{-2} corresponds to the device with 1.0 mol% Zn-doped TiO₂ photoanode. Zn is a n-type dopant, and hence, Zn doping increases the electron density in the conduction band of TiO₂, and thereby improves charge transport in the device [38]. A similar trend was observed in the present study up to 1.0 mol% of Zn content, but the charge transport was reduced with 1.5 and 2.0 mol% of dopant concentrations, maybe due to the recombination of electron-hole pairs. Jianping et al. reported on the formation of a shallow trapping centre of photo-generated carriers at low amounts of Zn dopant, which results in efficient separation of electron-hole pairs and long carrier lifetime and subsequent reduction in carrier recombination followed by rise in photocurrent. However, at higher amounts of Zn dopant, ZnO clusters onto the surface of TiO₂ by forming surface states. Hence, ZnO acts as a defect site and captures the electrons, which results in an increase in the recombination rate and causes a decrease in J_{sc} [38]. The present study exhibited an improved PCE of 5.67% for 1.0 mol% Zn-doped TiO₂ photoanode-based device, which was 35% higher than that of the control device fabricated with undoped TiO₂. This improvement in PCE is mainly attributed to the enhanced J_{sc} value; this observation was further confirmed by the EIS measurements.

2.4.2. Electrochemical Impedance Spectroscopy (EIS)

The EIS measurements were performed on the fabricated DSSCs by two electrode method at frequencies from 10^{-2} to 10^6 Hz in the dark, with a bias applied voltage of 10 mV. Figure 5 shows the Nyquist plot of the electrochemical impedance spectra of DSSCs fabricated with undoped and Zn-doped TiO_2 photoanodes.

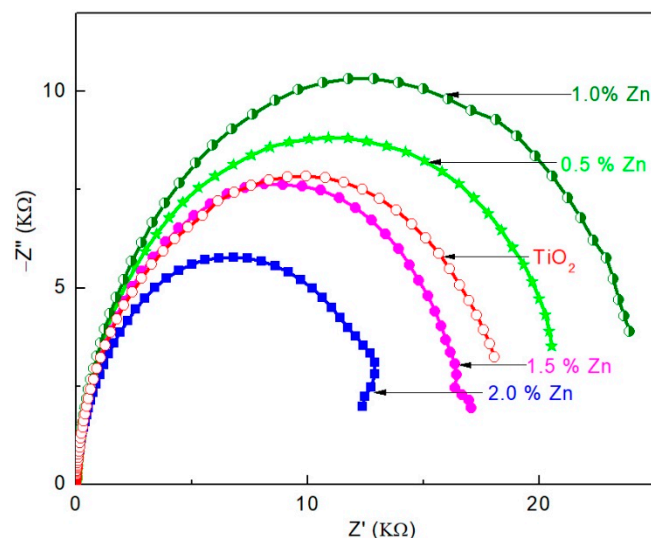


Figure 5. Nyquist plot of DSSCs with undoped, 0.5, 1.0, 1.5, and 2.0 mol% Zn-doped TiO_2 in dark.

As shown in the Figure 5, these Nyquist plots are related to the charge recombination resistance (R_2) across the TiO_2 /electrolyte interface, with a partial contribution from electron transport and accumulation in TiO_2 photoanode [39]. R_2 value of the undoped and Zn-doped TiO_2 photoanodes-based DSSCs can be estimated from the diameter of the respective semicircles [13]; a high R_2 value indicates low charge recombination rate [13,40]. In the present study, the R_2 value of undoped TiO_2 is lower than those of 0.5 and 1.0 mol% Zn-doped TiO_2 based DSSCs and higher than that of 1.5 and 2.0 mol% Zn-doped TiO_2 based device. Hence, the lowest charge recombination rate is attributed to the 1.0 mol% Zn-doped TiO_2 based device. These results are in good agreement with the J_{SC} values and the corresponding η values of the fabricated devices.

2.5. Photocatalytic Degradation Measurement

Photocatalytic degradation of MB using Zn-doped and undoped TiO_2 nanomaterials was performed under direct sunlight. Prior to the light exposure, the reaction suspension was allowed to establish adsorption-desorption equilibrium by stirring the suspension in dark for 30 min. Subsequently, the suspension was exposed to direct sunlight for a stipulated period (noon daytime) during which the MB retained in the suspension was measured at regular time intervals. The concentration of MB decreased with time, and the absorption peak corresponding to MB ($\lambda = 663$ nm) was found to disappear after 2.5 h. The concentration vs. time plots obtained for different Zn-doped TiO_2 (0.5, 1.0, 1.5, and 2.0 mol%) and undoped TiO_2 samples are depicted in Figure 6.

The MB dye was used as probing molecule to explore the photocatalytic degradation property of the synthesized nanomaterials. For the overall reaction, the zeroth order kinetic model with the optimum rate constant of $1.5466 \pm 0.0873 \times 10^{-4} \text{ s}^{-1}$ for TiO_2 doped 1.0% Zn doping (Table 3). There was a minimum 41% of increase in the activity while Zn was doped in 0.5% over bare TiO_2 . Moreover, the dark adsorption was carried out for 30 min to let the adsorption-desorption equilibrium be achieved, and during this process, the dye molecules are merely transferred from liquid stage to the solid state. With the absorbance vs. wavelength plot (as illustrated in Figure S1a) of dark adsorption studies, once the adsorption-desorption equilibrium is achieved, there is not much change in the

concentration of dye with time. However, the degradation occurs under the light exposure in the presence of catalyst (as illustrated in Figure S1b), and these results validate the contribution of catalyst in the dye degradation process. Further, the study without catalyst confirms that there is no self-degradation of dyes (as illustrated in Figure S1c). In summary, the catalysts used in this study are very effective against dye degradation in the presence of sunlight. Further, recycling study was carried out with 1% Zn-doped TiO₂ nanomaterial to examine its reusability. After the photocatalytic experiment, the catalyst was separated from the reaction mixture by centrifugation and used for 2nd cycle by following the same experimental conditions.

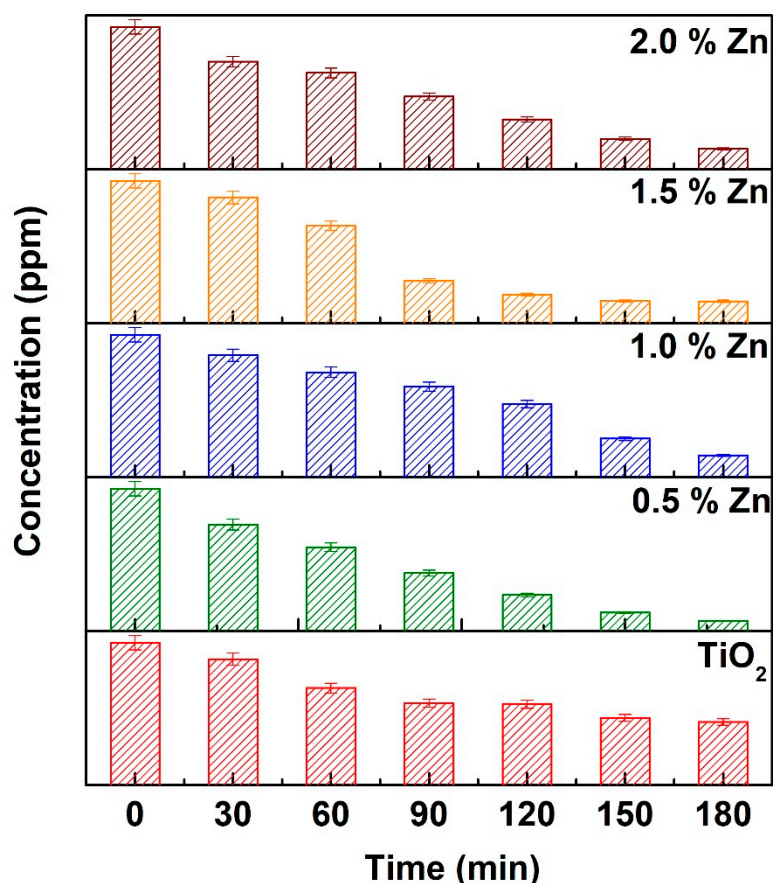


Figure 6. Concentration vs. time plot for degradation of methylene blue (MB) by undoped, 0.5, 1.0, 1.5, and 2.0 mol% Zn-doped TiO₂ as photocatalysts under direct sunlight.

Table 3. Overall rate constants for photocatalytic degradation of MB under direct sunlight with undoped, 0.5, 1.0, 1.5, and 2.0 mol% Zn-doped TiO₂ as photocatalysts.

Zn (mol%)	R-Square Value	Overall Rate Constant (K)
0.0	0.9035	$0.9533 \pm 0.1261 \times 10^{-4} \text{ s}^{-1}$
0.5	0.9207	$1.3416 \pm 0.1526 \times 10^{-4} \text{ s}^{-1}$
1.0	0.9812	$1.5466 \pm 0.0873 \times 10^{-4} \text{ s}^{-1}$
1.5	0.8764	$1.4833 \pm 0.2266 \times 10^{-4} \text{ s}^{-1}$
2.0	0.9749	$1.3533 \pm 0.0884 \times 10^{-4} \text{ s}^{-1}$

As shown in Figure 7, the photocatalyst did not exhibit any significant loss in the 2nd cycle of degradation of MB under the same conditions. The calculated degradation percentage were found to be 99% and 82% for 1st and 2nd use, respectively. The results confirm that the synthesized Zn-doped TiO₂ photocatalyst shows good stability and sus-

tainability. Moreover, the rate of the photocatalytic degradation results obtained in this study is compared with that of the literature and summarized in the Table 4.

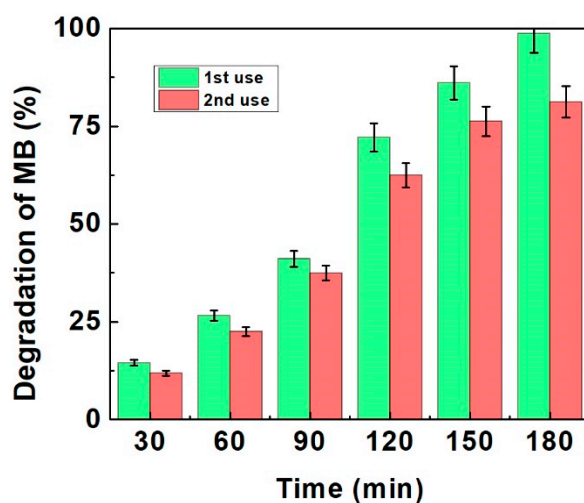


Figure 7. Reusability of optimized 1% Zn-doped TiO₂ nanomaterial.

Table 4. A comparison of photocatalytic degradation of MB by different doped/codoped TiO₂ nanomaterials.

Material	C ₀ (mg L ⁻¹)	Irradiation Time (min)	Catalyst Dose (g L ⁻¹)	Light Source	Degradation Efficiency (%)	Synthesis Method	Ref.
Pd/TiO ₂	20	120	1.0	UV, 100W	99.40	Sol-gel method	[41]
Ni/Cr co doped TiO ₂	5	90	2.0	Sunlight	95.60	Hydrothermal method	[5]
Doped TiO ₂					-		
C-TiO ₂					93.00–95.00		
Fe-TiO ₂					90.00		
N-TiO ₂					90.00		
Zn-TiO ₂					75.00–80.00		
Sb-TiO ₂	30	60	0.4	Sunlight	75.00–80.00	Sol-gel method	[42]
Sr-TiO ₂					75.00–80.00		
Ce-TiO ₂					75.00–80.00		
S-TiO ₂					75.00–80.00		
P-TiO ₂					75.00–80.00		
B-TiO ₂					75.00–80.00		
Co/TiO ₂	10	150	0.1	UV Visible	80.00 62.00	Sol-gel method	[43]
Mn/TiO ₂		180	1.0	Sunlight UV	96.90 76.35	Hydrothermal method	[44]
Fe/TiO ₂	100	65	0.5	300 W mercury vapor lamp (365 nm)	72.20	Hydrothermal method	[45]
Zn/TiO ₂	10	180	0.5	Sunlight	99.15	Solvothermal method	This work

Although the experimental conditions and other factors vary, based on the summary of the table, our proposed synthesised nanomaterials effectively degrade the MB under the sunlight compared to that of the other reports. Therefore, this cost effective solvothermal method is preferable for the synthesis of nanomaterials for energy and environmental applications.

3. Materials and Methods

3.1. Materials

Absolute ethanol (>99%), Triton X-100, Zinc acetate dihydrate ($\geq 98\%$), Titanium tetraisopropoxide (TTIP, >98%), Di-tetrabutylammonium cis-bis (isothiocyanato)bis(2,2'-bipyridyl-4,4'-dicarboxylato) ruthenium (II) dye (95%), Acetonitrile, Tert-butyl alcohol ($\geq 99.7\%$), and MB (95%) were purchased from Sigma–Aldrich, Oslo, Norway AS. Acetylacetone ($\geq 99.5\%$) was purchased from Fluka Analytical, Munich, Germany. All the materials were used without further purification.

3.2. Methodology

3.2.1. Synthesis of Zn-Doped and Undoped TiO₂ Nanomaterials

A 3 mL mixture of TTIP and ethanol in 1:16 volume ratio was vigorously stirred in a 50 mL reaction bottle. Appropriate amounts of Zn(CH₃COO)₂·2H₂O were then added separately to the above solution to prepare different photocatalysts with 0.5, 1.0, 1.5, and 2.0 mol% Zn, and the resultant mixtures were stirred well for one hour. Subsequently, a solution containing ethanol and deionized water in 1:1 volume ratio was added separately to the above mixtures. A white color precipitate was attained after addition of ethanol-water mixture. Then, the products were sintered at 90 °C for 6 h, dried at 100 °C to get powder samples, and subsequently calcinated at 500 °C for 2 h to obtain 0.5, 1.0, 1.5, and 2.0 mol% Zn-doped TiO₂ nanomaterials [46]. The undoped TiO₂ was synthesized by adopting the same procedure without employing Zn(CH₃COO)₂·2H₂O.

3.2.2. Device Fabrication

The Fluorine doped Tin Oxide (FTO) coated glass substrates (Sigma–Aldrich surface resistivity 7.5 Ω/cm²) were cleaned in ultrasonic bath for 10 min with soap water, distilled water and ethanol, successively. The synthesized undoped and Zn-doped TiO₂ nanomaterials were coated separately on cleaned FTO substrates by doctor-blade method. Then, the resultant films were calcinated at 500 °C for 30 min and soaked in 0.3 mM solution of N719 dye and prepared in a mixture of acetonitrile and tert-butyl alcohol [46,47] for 12 h. Afterwards, the dye coated films were rinsed in acetonitrile and subsequently dried. The platinum (Pt) coated glass substrate [48] was assembled with each dye-coated photoanode as counter electrode. Finally, a small amount of I⁻/I₃⁻ electrolyte was injected in between the dye coated photoanode and Pt counter electrode to complete the fabrication of DSSC.

3.2.3. Photocatalytic Degradation

Photocatalytic degradation of MB solution was performed using undoped and 0.5, 1.0, 1.5, and 2.0 mol% Zn-doped TiO₂ nanomaterials. As reported in our previous study [49], 25.0 mg of the photocatalyst was suspended in 50 mL of MB solution (initial concentration was 10 ppm) under direct sunlight (intensity of ~100 mWcm⁻²). Prior to irradiation, the MB solution with photocatalyst was stirred in the dark for 30 min to ensure the establishment of adsorption or desorption equilibrium. Periodically, 3 mL of suspension was withdrawn and centrifuged, and its absorbance was obtained using UV-visible spectrophotometer (JENWAY 6800, OSA, UK).

3.3. Characterization

The structural properties of the synthesized nanomaterials were studied by the X-ray diffraction method (PANalytical-AERIS, Almelo, The Netherland) using scan range (2θ) between 20–90° with step size of 0.02° and scan speed of 1°/min. The optical absorbance spectra were recorded using Shimadzu 1800 Scanning Double Beam UV-visible spectrophotometer. The elemental composition of the synthesized nanomaterials was analyzed by the energy-dispersive X-ray spectroscopy technique. The photovoltaic performance of the cells was studied using Keithley-2400 source measurement unit (SMU) under simulated irradiation by 150 W Xe lamp of intensity 100 mWcm⁻² with AM 1.5 filter (Peccell-PEC-L12, Kanagawa, Japan), and the effective area of the devices is 0.25 cm². Elec-

trochemical impedance spectroscopy (EIS) measurements were carried out on the DSSCs using Metrohm Autolab potentiostat/galvanostat (PGSTAT 128N, Utrecht, Netherlands) with a frequency response analyzer (FRA 32M).

4. Conclusions

In the present study, undoped and Zn-doped TiO₂ nanomaterials were synthesized by a simple solvothermal method and characterized. The XRD study revealed the existence of anatase phase without any phase transformation in all the synthesized nanomaterials. The UV-visible spectra of Zn-doped TiO₂ nanomaterials demonstrated red shift compared to that of the spectrum of undoped TiO₂. The EDX spectroscopy confirmed the inclusion of Zn element in the Zn-doped TiO₂ nanomaterials. The photovoltaic performances of DSSCs fabricated with the synthesized undoped and Zn-doped nanomaterials were analyzed; 1.0 mol% Zn-doped TiO₂ based device exhibited PCE of 5.67%, which was greater than 35% enhancement compared to that of the control device due to increased J_{SC}. Moreover, 1.0 mol% Zn-doped TiO₂ displayed efficient photocatalytic property in the degradation of MB under direct sun light. The improved performance revealed by the 1.0 mol% Zn-doped TiO₂ nanomaterials in both photovoltaic and photocatalytic applications could be attributed to its reduced charge recombination rate and enhanced visible light harvesting ability.

Supplementary Materials: The following are available online at <https://www.mdpi.com/article/10.3390/catal11060690/s1>, **Figure S1.** Absorbance vs. wavelength plot for (a) methylene blue with catalyst [1.0 mol% Zn-TiO₂] under dark condition (b) methylene blue with catalyst [1.0 mol% Zn-TiO₂] in the presence of light (c) photolysis of methylene blue without catalyst in the presence of light.

Author Contributions: Conceptualization, T.R., S.S., V.G and S.Y.; methodology, T.R., S.S., V.G. and S.Y.; software, T.R. and S.S.; validation, T.R., S.S., S.Y., D.V., P.R. and M.S.; formal analysis, T.R., V.G and S.S.; investigation, T.R., S.S. and S.Y.; resources, D.V., P.R.; data curation, T.R., S.S., S.Y., D.V., P.R. and M.S.; writing—original draft preparation, T.R. and S.S.; writing—review and editing, S.Y. and M.S.; supervision, S.Y., D.V., P.R. and M.S.; project administration, D.V. and P.R.; funding acquisition, D.V. and P.R. All authors have read and agreed to the published version of the manuscript.

Funding: This research was funded by Capacity Building and Establishment of a Research Consortium (CBERC) project, grant number LKA-3182-HRNCET, and Higher Education and Research collaboration on Nanomaterials for Clean Energy Technologies (HRNCET) project, grant number NORPART/2016/10237.

Data Availability Statement: Data available in a publicly accessible repository.

Conflicts of Interest: The authors declare no conflict of interest. The funders had no role in the design of the study; in the collection, analyses, or interpretation of data; in the writing of the manuscript, or in the decision to publish the results.

References

1. Perera, F. Pollution from fossil-fuel combustion is the leading environmental threat to global pediatric health and equity: Solutions exist. *Int. J. Environ. Res. Public Health* **2018**, *15*, 16. [[CrossRef](#)]
2. Owusu, P.A.; Asumadu-Sarkodie, S. A review of renewable energy sources, sustainability issues and climate change mitigation. *Cogent Eng.* **2016**, *3*, 1–14. [[CrossRef](#)]
3. Nyankson, E.; Agyei-Tuffour, B.; Asare, J.; Annan, E.; Rwenyagila, E.R.; Konadu, D.S.; Yaya, A.; Doodoo-Arhin, D. Nanostructured TiO₂ and their energy applications—A review. *ARN J. Eng. Appl. Sci.* **2013**, *8*, 871–886.
4. Chen, S.; Li, L.; Sun, H.; Sun, J.; Lu, B. Nanomaterials for renewable energy. *J. Nanomater.* **2015**, *2015*, 2–4. [[CrossRef](#)]
5. Shaban, M.; Ahmed, A.M.; Shehata, N.; Betiha, M.A.; Rabie, A.M. Ni-doped and Ni/Cr co-doped TiO₂ nanotubes for enhancement of photocatalytic degradation of methylene blue. *J. Colloid Interface Sci.* **2019**, *555*, 31–41. [[CrossRef](#)]
6. Lü, X.; Xia, B.; Liu, C.; Yang, Y.; Tang, H. TiO₂-Based Nanomaterials for Advanced Environmental and Energy-Related Applications. *J. Nanomater.* **2016**, *2016*. [[CrossRef](#)]
7. Moma, J.; Baloyi, J. Modified titanium dioxide for photocatalytic applications. In *Photocatalysts—Applications and Attributes*; Intechopen: London, UK, 2019; Volume 18.
8. Aduda, B.O.; Ravirajan, P.; Choy, K.L.; Nelson, J. Effect of morphology on electron drift mobility in porous TiO₂. *Int. J. Photoenergy* **2004**, *6*, 141–147. [[CrossRef](#)]

9. Kajana, T.; Velauthapillai, D.; Shivatharsiny, Y.; Ravirajan, P.; Yuvapragasam, A.; Senthilnathanan, M. Structural and photoelectrochemical characterization of heterostructured carbon sheet/Ag₂MoO₄-SnS/Pt photocapacitor. *J. Photochem. Photobiol. A Chem.* **2020**, *401*, 112784. [[CrossRef](#)]
10. Shanmugaratnam, S.; Velauthapillai, D.; Ravirajan, P.; Christy, A.A.; Shivatharsiny, Y. CoS₂/TiO₂ Nanocomposites for Hydrogen Production under UV Irradiation. *Materials* **2019**, *12*, 3882. [[CrossRef](#)] [[PubMed](#)]
11. Zhang, L.; Qin, M.; Yu, W.; Zhang, Q.; Xie, H.; Sun, Z.; Shao, Q.; Guo, X.; Hao, L.; Zheng, Y. Heterostructured TiO₂/WO₃ nanocomposites for photocatalytic degradation of toluene under visible light. *J. Electrochem. Soc.* **2017**, *164*, H1086. [[CrossRef](#)]
12. Muduli, S.; Game, O.; Dhas, V.; Vijayamohan, K.; Bogle, K.A.; Valanoor, N.; Ogale, S.B. TiO₂-Au plasmonic nanocomposite for enhanced dye-sensitized solar cell (DSSC) performance. *Sol. Energy* **2012**, *86*, 1428–1434. [[CrossRef](#)]
13. Rajaramanan, T.; Natarajan, M.; Ravirajan, P.; Senthilnathanan, M.; Velauthapillai, D. Ruthenium (Ru) Doped Titanium Dioxide (P25) electrode for dye sensitized solar cells. *Energies* **2020**, *13*, 1532. [[CrossRef](#)]
14. Tanyi, A.R.; Rafieh, A.I.; Ekaneyaka, P.; Tan, A.L.; Young, D.J.; Zheng, Z.; Chellappan, V.; Subramanian, G.S.; Chandrakanthi, R.L.N. Enhanced efficiency of dye-sensitized solar cells based on Mg and La co-doped TiO₂ photoanodes. *Electrochim. Acta* **2015**, *178*, 240–248. [[CrossRef](#)]
15. Madurai Ramakrishnan, V.; Natarajan, M.; Pitchaiya, S.; Santhanam, A.; Velauthapillai, D.; Pugazhendhi, A. Microwave assisted solvothermal synthesis of quasi cubic F doped TiO₂ nanostructures and its performance as dye sensitized solar cell photoanode. *Int. J. Energy Res.* **2020**, 1–10. [[CrossRef](#)]
16. Feng, T.; Feng, G.S.; Yan, L.; Pan, J.H. One-dimensional nanostructured TiO₂ for photocatalytic degradation of organic pollutants in wastewater. *Int. J. Photoenergy* **2014**, *2014*, 563879. [[CrossRef](#)]
17. Roose, B.; Pathak, S.; Steiner, U. Doping of TiO₂ for sensitized solar cells. *Chem. Soc. Rev.* **2015**. [[CrossRef](#)]
18. Huang, F.; Li, Q.; Thorogood, G.J.; Cheng, Y.-B.; Caruso, R.A. Zn-doped TiO₂ electrodes in dye-sensitized solar cells for enhanced photocurrent. *J. Mater. Chem.* **2012**, *22*, 17128–17132. [[CrossRef](#)]
19. Singla, P.; Sharma, M.; Pandey, O.P.; Singh, K. Photocatalytic degradation of azo dyes using Zn-doped and undoped TiO₂ nanoparticles. *Appl. Phys. A* **2013**. [[CrossRef](#)]
20. Zhao, Y.; Li, C.; Liu, X.; Gu, F.; Du, H.L.; Shi, L. Zn-doped TiO₂ nanoparticles with high photocatalytic activity synthesized by hydrogen-oxygen diffusion flame. *Appl. Catal. B Environ.* **2008**, *79*, 208–215. [[CrossRef](#)]
21. Tariq, M.K.; Riaz, A.; Khan, R.; Wajid, A.; Haq, H.-U.; Javed, S.; Akram, M.A.; Islam, M. Comparative study of Ag, Sn or Zn doped TiO₂ thin films for photocatalytic degradation of methylene blue and methyl orange. *Mater. Res. Express* **2019**, *6*, 106435. [[CrossRef](#)]
22. Zhu, F.; Zhang, P.; Wu, X.; Fu, L.; Zhang, J.; Xu, D. The Origin of Higher Open-Circuit Voltage in Zn-Doped TiO₂ Nanoparticle-Based Dye-Sensitized Solar Cells. *ChemPhysChem* **2012**, *13*, 3731–3737. [[CrossRef](#)]
23. Chen, C.; Wang, Z.; Ruan, S.; Zou, B.; Zhao, M.; Wu, F. Photocatalytic degradation of CI Acid Orange 52 in the presence of Zn-doped TiO₂ prepared by a stearic acid gel method. *Dye. Pigment.* **2008**, *77*, 204–209. [[CrossRef](#)]
24. Yang, G.; Jiang, Z.; Shi, H.; Jones, M.O.; Xiao, T.; Edwards, P.P.; Yan, Z. Study on the photocatalysis of F-S co-doped TiO₂ prepared using solvothermal method. *Appl. Catal. B Environ.* **2010**, *96*, 458–465. [[CrossRef](#)]
25. Okuya, M.; Nakade, K.; Kaneko, S. Porous TiO₂ thin films synthesized by a spray pyrolysis deposition (SPD) technique and their application to dye-sensitized solar cells. *Sol. Energy Mater. Sol. Cells* **2002**, *70*, 425–435. [[CrossRef](#)]
26. Ding, K.; Miao, Z.; Liu, Z.; Zhang, Z.; Han, B.; An, G.; Miao, S.; Xie, Y. Facile Synthesis of High Quality TiO₂ Nanocrystals in Ionic Liquid via a Microwave-Assisted Process. *J. Am. Chem. Soc.* **2007**, *129*, 6362–6363. [[CrossRef](#)]
27. Elfanaoui, A.; Elhamri, E.; Boulkaddat, L.; Ihlal, A.; Bouabid, K.; Laanab, L.; Taleb, A.; Portier, X. Optical and structural properties of TiO₂ thin films prepared by sol-gel spin coating. *Int. J. Hydrogen Energy* **2011**, *36*, 4130–4133. [[CrossRef](#)]
28. Shahid, M.; McDonagh, A.; Salim, A.P.; Kim, J.H.; Shon, H.K. Magnetised Titanium Dioxide (TiO₂) for Water Purification: Preparation, Characterisation, and Application. *Desalination Water Treat.* **2015**, *54*, 979–1002. [[CrossRef](#)]
29. Loan, T.T.; Huong, V.H.; Tham, V.T.; Long, N.N. Effect of zinc doping on the bandgap and photoluminescence of Zn²⁺-doped TiO₂ nanowires. *Phys. B Condens. Matter* **2018**, *532*, 210–215. [[CrossRef](#)]
30. Kumar, S.; Das, B. Effect of lattice strain on X-ray Diffraction, Raman Spectroscopy and Optical Properties of as Synthesis Nanocomposite ZnO-SnO₂-TiO₂ Thin Film by Spray Pyrolysis Method. *Semant. Sch.* **2017**, *2017*, 5204639.
31. Alikhanov, N.M.-R.; Rabadanov, M.K.; Orudzhev, F.F.; Gadzhimagomedov, S.K.; Emirov, R.M.; Sadykov, S.A.; Kallaev, S.N.; Ramazanov, S.M.; Abdulvakhidov, K.G.; Sobola, D. Size-dependent structural parameters, optical, and magnetic properties of facile synthesized pure-phase BiFeO₃. *J. Mater. Sci. Mater. Electron.* **2021**, 1–13. [[CrossRef](#)]
32. Prabu, K.M.; Perumal, S. Micro Strain and Morphological Studies of Anatase and Rutile Phase TiO₂ Nanocrystals Prepared via Sol-Gel and Solvothermal Method—A Comparative Study. *IJSRSET* **2015**, *1*, 299–304.
33. Moghaddam, H.M.; Nasirian, S. Dependence of activation energy and lattice strain on TiO₂ nanoparticles? *Nanosci. Methods* **2012**, *1*, 201–212. [[CrossRef](#)]
34. Lv, Y.; Tong, H.; Cai, W.; Zhang, Z.; Chen, H.; Zhou, X. Boosting the efficiency of commercial available carbon-based perovskite solar cells using Zinc-doped TiO₂ nanorod arrays as electron transport layer. *J. Alloy. Compd.* **2021**, *851*, 156785. [[CrossRef](#)]
35. Wang, Y.; Zhang, R.; Li, J.; Li, L.; Lin, S. First-principles study on transition metal-doped anatase TiO₂. *Nanoscale Res. Lett.* **2014**, *9*, 46. [[CrossRef](#)]

36. Arunachalam, A.; Dhanapandian, S.; Manoharan, C.; Sivakumar, G. Physical properties of Zn doped TiO₂ thin films with spray pyrolysis technique and its effects in antibacterial activity. *Spectrochim. Acta-Part A Mol. Biomol. Spectrosc.* **2015**, *138*, 105–112. [[CrossRef](#)] [[PubMed](#)]
37. Aware, D.V.; Jadhav, S.S. Synthesis, characterization and photocatalytic applications of Zn-doped TiO₂ nanoparticles by sol-gel method. *Appl. Nanosci.* **2016**, *6*, 965–972. [[CrossRef](#)]
38. Deng, J.; Wang, M.; Fang, J.; Song, X.; Yang, Z.; Yuan, Z. Synthesis of Zn-doped TiO₂ nano-particles using metal Ti and Zn as raw materials and application in quantum dot sensitized solar cells. *J. Alloy. Compd.* **2019**, *791*, 371–379. [[CrossRef](#)]
39. Mehnane, H.F.; Wang, C.; Kondamareddy, K.K.; Yu, W.; Sun, W.; Liu, H.; Bai, S.; Liu, W.; Guo, S.; Zhao, X. Hydrothermal synthesis of TiO₂ nanoparticles doped with trace amounts of strontium, and their solar cells: Tunable electrical properties & enhanced photo-conversion performance. *RSC Adv.* **2017**, 2358–2364. [[CrossRef](#)]
40. Madurai Ramakrishnan, V.; Muthukumarasamy, N.; Balraju, P.; Pitchaiya, S.; Velauthapillai, D.; Pugazhendhi, A. Transformation of TiO₂ nanoparticles to nanotubes by simple solvothermal route and its performance as dye-sensitized solar cell (DSSC) photoanode. *Int. J. Hydrogen Energy* **2020**, *45*, 15441–15452. [[CrossRef](#)]
41. Nguyen, C.H.; Fu, C.C.; Juang, R.S. Degradation of methylene blue and methyl orange by palladium-doped TiO₂ photocatalysis for water reuse: Efficiency and degradation pathways. *J. Clean. Prod.* **2018**, *202*, 413–427. [[CrossRef](#)]
42. Bhosale, R.R.; Pujari, S.R.; Muley, G.G.; Patil, S.H.; Patil, K.R.; Shaikh, M.F.; Gambhire, A.B. Solar photocatalytic degradation of methylene blue using doped TiO₂ nanoparticles. *Sol. Energy* **2014**, *103*, 473–479. [[CrossRef](#)]
43. Pirbazari, A.E.; Monazzam, P.; Kisomi, B.F. Co/TiO₂ nanoparticles: Preparation, characterization and its application for photocatalytic degradation of methylene blue. *Desalin. Water Treat.* **2017**, *63*, 283–292. [[CrossRef](#)]
44. Shahmoradi, B.; Negahdary, M.; Maleki, A. Hydrothermal synthesis of surface-modified, manganese-doped TiO₂ nanoparticles for photodegradation of methylene blue. *Environ. Eng. Sci.* **2012**, *29*, 1032–1037. [[CrossRef](#)]
45. Li, Z.; Shen, W.; He, W.; Zu, X. Effect of Fe-doped TiO₂ nanoparticle derived from modified hydrothermal process on the photocatalytic degradation performance on methylene blue. *J. Hazard. Mater.* **2008**, *155*, 590–594. [[CrossRef](#)]
46. Madurai Ramakrishnan, V.; Pitchaiya, S.; Muthukumarasamy, N.; Kvamme, K.; Rajesh, G.; Agilan, S.; Pugazhendhi, A.; Velauthapillai, D. Performance of TiO₂ nanoparticles synthesized by microwave and solvothermal methods as photoanode in dye-sensitized solar cells (DSSC). *Int. J. Hydrogen Energy* **2020**, *45*, 27036–27046. [[CrossRef](#)]
47. Pirashanthan, A.; Murugathas, T.; Robertson, N.; Ravirajan, P.; Velauthapillai, D. A Quarterthiophene-Based Dye as an Efficient Interface Modifier for Hybrid Titanium Dioxide/Poly(3-hexylthiophene)(P3HT) Solar Cells. *Polymers* **2019**, *11*, 1752. [[CrossRef](#)]
48. Wijayarathna, T.R.C.K.; Aponsu, G.M.L.P.; Ariyasinghe, Y.P.Y.P.; Premalal, E.V.A.; Kumara, G.K.R.; Tennakone, K. A high efficiency indoline-sensitized solar cell based on a nanocrystalline TiO₂ surface doped with copper. *Nanotechnology* **2008**, *19*, 485703. [[CrossRef](#)] [[PubMed](#)]
49. Shanmugaratnam, S.; Selvaratnam, B.; Baride, A.; Koodali, R. SnS₂/TiO₂ Nanocomposites for Hydrogen Production and Photodegradation Under Extended Solar Irradiation. *Catalysts* **2021**, *11*, 589. [[CrossRef](#)]